



MIT Open Access Articles

Sensor modeling for the virtual autonomous navigation environment

The MIT Faculty has made this article openly available. **Please share** how this access benefits you. Your story matters.

Citation	Goodin, C. et al. "Sensor modeling for the Virtual Autonomous Navigation Environment." Sensors, 2009 IEEE. 2009. 1588-1592. © 2010 Institute of Electrical and Electronics Engineers.
As Published	http://dx.doi.org/10.1109/ICSENS.2009.5398491
Publisher	Institute of Electrical and Electronics Engineers
Version	Final published version
Accessed	Tue Apr 24 15:38:52 EDT 2018
Citable Link	http://hdl.handle.net/1721.1/59345
Terms of Use	Article is made available in accordance with the publisher's policy and may be subject to US copyright law. Please refer to the publisher's site for terms of use.
Detailed Terms	

Sensor Modeling for the Virtual Autonomous Navigation Environment

Chris Goodin, Raju Kala, Alex Carrillo
Engineer Research and Development Center
Vicksburg, MS 39180
Email: christopher.t.goodin@usace.army.mil

Linda Y. Liu
Department of Mechanical Engineering
Massachusetts Institute of Technology
Cambridge, MA 02139

Abstract—The Virtual Autonomous Navigation Environment (VANE) is a high fidelity, physics-based simulation process that produces realistic simulated sensor output for use in the development and testing of Autonomous Mobility Systems (AMS). The VANE produces simulated sensor output for ranging and camera sensors that are characterized by a few easily determined input parameters. This flexibility allows for the efficient characterization of a sensor interaction with a particular AMS. This paper presents the development of these models and some initial results.

I. INTRODUCTION

The VANE is currently being developed by the U.S. Army Engineer Research and Development Center. The VANE is intended to provide a realistic simulated environment for testing AMS on unmanned ground vehicles. Physics-based sensor, thermal, vehicle-terrain interaction, groundwater, and reflectance models will be incorporated into the VANE. Fig. 1 shows the VANE simulation concept, with the sensor model piece shown in the bottom middle box.

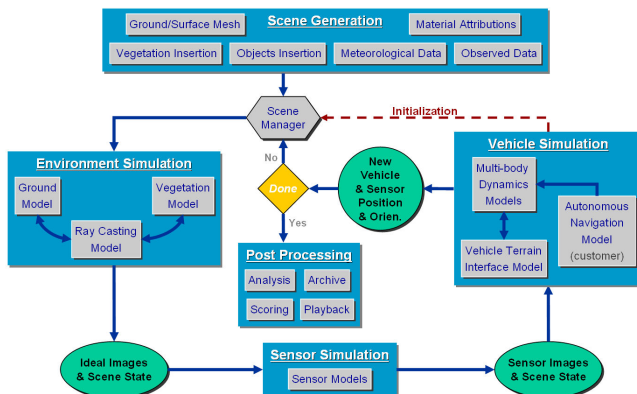


Fig. 1. The VANE simulation concept.

While VANE must produce high fidelity simulated sensor data, the sensor models must also be efficient and flexible because of the intended use of the VANE. As shown in the right side of Fig. 1, the primary customers of the VANE are AMS developers. To make the VANE tools open and accessible to these customers, the sensor models should not require a highly detailed characterization of each sensor. Instead, the model should take a few easily measurable parameters as input.

Furthermore, since a typical VANE simulation may produce hundreds or even thousands of images, as well as perhaps tens of thousands of LIDAR pulses, the software models should be developed with a minimum level of computational requirements.

With these goals and limitations in mind, Light Detection and Ranging (LIDAR) and Charge Coupled Device (CCD) models have been developed to serve as the primary sensor models in the VANE. Both models are somewhat generic in that they take simple parameters describing the geometry and/or optics of the system, as well as the sensor responses and electronic processing, as input. Both the LIDAR and CCD models are described in this work.

II. THE QUICK CASTER

Ideal images of scenes in the VANE are produced with a ray caster, called the Quick Caster (QC), that was developed to provide input to a variety of sensor applications within the framework of a large scale computational test bed [1]. The QC program uses ray casting techniques to provide the necessary scene information to the visual CCD camera models and the LIDAR sensor models. The QC uses the triangular facets from the meshes used by the various physics-based models to define the scene geometry. Other material properties (color, temperature, reflectance, *etc.*) can be assigned by either node or facet. Since highly detailed scenes can potentially exceed several billion facets, the QC program is parallelized by facet rather than the typical parallelization by ray, and is fully distributed and scalable on large distributed memory computers.

III. CCD MODEL

The CCD sensor model used in VANE is similar to that outlined by [2] in that the image is processed in a sequential manner to account for the camera filter, optical system, vignetting, field stop, CCD response function, and exposure time. However, while [2] calculate the point spread function to characterize the optical system, the VANE sensor model uses a geometrical optics ray-tracing method to trace each ray through the optical system. In principle, these methods should produce identical results as long as the spatial sampling of the geometrical method has a high resolution. Each of the

sequential operations that map the ideal image from the QC to a synthetic sensor image is described below.

A. Filter Functions and CCD Spectral Response

The QC can track up to six unique user defined spectral bands during a simulation. For a red-green-blue (RGB) color camera, the width and center of the red, green, and blue bands are defined by the properties of the CCD color filters. The CCD filter functions are applied to the input light in pre-processing. The power density of the input light spectrum is integrated over the filter function for each band. The filter functions shown in Fig. 2 are for the Point Grey Bumblebee CCD camera, which uses a Sony ICX204 color CCD sensor. The filter function and the spectral response for this camera are given as one curve in the data sheet. However, if they were separate, the integral for each band would simply be integrated with both the filter and the spectral response as weighting functions.

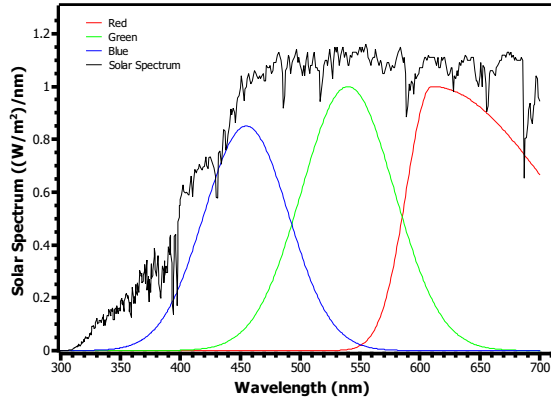


Fig. 2. Example of filter functions for the Bumblebee RGB cameras.

B. Geometrical Optical Model

For a pinhole camera model with a given focal length f , it is straightforward to create an ideal image for an unaberrated system. If the imaging system is not ideal (as is always the case to some degree), then there will be some defocus and possibly other aberrations that must be accounted for in the aberration function. For an object at (x_o, y_o, z_o) , where the origin is at the center of the camera pupil and $+z$ is in the direction of the object and perpendicular to the pupil plane, the general aberration function can be expanded in even powers of the coordinates (x_o, y_o) and (x_p, y_p) , where (x_p, y_p) are the pupil coordinates. Discarding terms of order six and higher gives the aberration function with the primary Seidel aberrations, defined by [3]

$$W(x_o, y_o; x_p, y_p) = Ap^2 + B\rho^4 + C\kappa^4 + Dr^2\rho^2 + Er^2\kappa^2 + F\rho^2\kappa^2 \quad (1)$$

where

$$r^2 = x_o^2 + y_o^2, \quad \rho^2 = x_p^2 + y_p^2, \quad \kappa^2 = x_o x_p + y_o y_p \quad (2)$$

and A =defocus, B =spherical aberration, C =astigmatism, D =curvature, E =distortion, and F =coma. According to [4], the defocus parameter, A can be estimated by

$$A = \frac{a^2}{2r_o} \frac{r_o - s}{s} \quad (3)$$

where a is the radius of the exit pupil, r_o is the object distance, and s is the in-focus distance, given by

$$s = \left(\frac{1}{f} - \frac{1}{d} \right)^{-1} \quad (4)$$

where d is the distance from the exit pupil to the image plane.

Given the Seidel parameters, the deviation from the ideal image coordinates, (x_i, y_i) can be approximated from the aberration function by

$$\Delta x = x_i - x_o = -R_i \frac{\partial W}{\partial x_p}, \quad \Delta y = y_i - y_o = -R_i \frac{\partial W}{\partial y_p} \quad (5)$$

where R_i is approximated as the distance from the exit pupil to the ideal image plane. To be exact, R_i should be taken as the distance from the image plane to the aberrated wavefront emerging from the exit pupil, but the error in this approximation is small if the aberrations are small compared to the distance R_i , as is the case for commercially available cameras. Furthermore, (5) assumes the image space is filled with air, for which the index of refraction is ≈ 1 .

According to (1), input for the sensor model consists of not only an ideal image but also the geometry of the scene in question. Therefore, the QC calculates a 2000×2000 array of the distance to the object from each pixel. From this, $(\Delta x, \Delta y)$ values are calculated and applied to the ideal image. The (x_i, y_i) locations of the transformed points are interpolated to a grid representing the CCD pixel array with nearest neighbor interpolation, and the points that fall outside the field stop are disregarded. The virtual grid can be equal to the resolution of the pixel grid or greater than the resolution by a factor of an integer. For a typical CCD array of 1024×768 (for example, the Sony ICX204), a sample factor of 3 or more is possible from a 2000×2000 ideal image. The energy falling on each pixel is determined by integrating the irradiance over the area of the pixel, with the number of integration steps equal to the square of the sample factor.

C. Pixel Vignetting, Gain, and Gamma setting

Pixel vignetting, which is unique to CCD cameras, is caused by the lower incident angle of the light on pixels near the edge of the array, resulting in a darkening of the image near the edges. The vignetting function, $V(x_i, y_i)$ used for this model is given by [5]

$$V(x_i, y_i) = (1 - \alpha r) \left(\frac{f}{\sqrt{f^2 + x_i^2 + y_i^2}} \right)^4 \quad (6)$$

with α as a parameter describing the optical properties of the multi-lens system. Note that *tilt* term from [5] has been neglected in this model because it is not relevant for imaging scenes with great variations in depth. After the vignetting

function is applied to the image, all the pixels are multiplied by the gain setting and raised to the gamma. The real numbers are rounded to integers to produce the final RGB image.

D. Inputs to the CCD model

The CCD model requires an input file with a few relatively easily determined parameters. The parameters describing the geometry of the physical camera are the distance from the exit pupil to the CCD array, the dimensions of the CCD array, and the number of pixels in the CCD array. The optical system is described by the focal length, the radius of the entrance pupil, the exposure time, the gamma setting, the vignetting parameter, and the five primary Seidel aberrations. Finally, the CCD electronics are described by a gain factor, which may or may not have a chromatic dependence. Therefore, there are 16 independent parameters required to fully describe the model.

IV. LIDAR MODEL

As mentioned above, the geometric optics model takes an array of distances to facets in the scene as input. This distance array can also be used as input for the LIDAR model. In this model, the beam is represented by the diverging rays passing from a virtual focal point located several meters behind the sensor, through an image plane, and into the scene. The intersections of these rays with facets in the scene are found, and a return signal is calculated for each ray based on the solid angle of the detector relative to the facet and the reflectance properties of the facet. The contribution of each ray to the final signal is put into a time histogram, with the bins size determined by the time resolution of the sensor electronics.

The model presented here is roughly representative of the Sick LMS-291, for which mathematical models have previously been developed by [6] and [7], although the parameters of our model are variable and somewhat arbitrary since we have not fully characterized the sensor. Our model differs from these in that we use ray-tracing through an ideal-image plane to define the laser pulse shape and emittance by using a virtual focal length and detector dimensions.

A. Beam Divergence

The divergence of a circular beam can be simulated by tracing rays from a focal point through an ideal image plane and finding intersections of the rays with facets. A circular beam with a radius r at the aperture and a divergence Θ , the beam is simulated as a collection of rays passing through an $2r \times 2r$ image plane with a focal length, f , given by

$$f = \frac{r}{\tan(\frac{\Theta}{2})} \quad (7)$$

For a circular beam, the rays in the square image plane that lie outside the beam radius are ignored, yielding a circular diverging beam. The example shown in this paper is for a beam with a divergence of 10 mrad and a spot diameter of 2.5 cm at the exit aperture. This gives a focal length of 2.5 m.

The ray tracing method through an ideal image plane approximates the divergence of a continuous beam as a set of discrete rays. The reflected intensity of each ray is added

to the resulting pulse to reproduce the signal made by a continuous beam. The number N of discrete rays in one dimension necessary to realistically reproduce a continuous signal depends on the spatial resolution of the beam at the target x , the aperture radius r , the maximum range R_{max} , and the divergence of the beam Θ

$$N = \frac{2(r + R \tan(\frac{\Theta}{2}))}{x} \quad (8)$$

The necessary spatial resolution has been determined empirically through repeated trials using several geometries. The pulse vs time signals were compared for varying spatial resolutions at the target. The shape of the return pulse varied as the number of pixels was increased up to a certain point; beyond that point increases to the resolution did not affect the pulse shape. Therefore, this characteristic resolution, which is about 1 cm at a distance of 80 m, is the lowest threshold on resolution for simulating a laser pulse with the ideal image method. The characteristic spatial resolution threshold is obviously dependent on the time resolution; the detector tested in this example was assumed to have a 0.5 ns time step.

B. Beam Profile

The LIDAR model presented here assumes a Gaussian beam profile, for which the intensity as a function of radius r from the center of the beam spot and distance z from the aperture is

$$I(r, z) = I_0 \left(\frac{\omega_0}{\omega(z)} \right)^2 \exp\left(\frac{-2r^2}{\omega^2(z)} \right) \quad (9)$$

where $z_r = \pi \omega_0^2 / \lambda$ and $\omega_0 = \lambda / (\pi \Theta)$, where λ is the wavelength of the laser. The value of I_0 is found by integrating 9 over r and setting the result equal to the laser power, P .

$$I_0 = \frac{2P}{\pi \omega_0^2} \quad (10)$$

and $\omega(z)$ is given by

$$\omega(z) = \omega_0 \sqrt{1 + \left(\frac{z}{z_r} \right)^2} \quad (11)$$

The maximum intensity of the Gaussian profile decreases as $\approx 1/(1+z^2)$, so the intensity of the return decreases drastically with increasing distance.

C. Inputs to the LIDAR model

The LIDAR model takes twelve parameters as input, similar to the parameterization used by [8]. The parameters describing the laser pulse are the peak laser power, the beam radius at the exit aperture, the wavelength of the laser, and the pulse duration. The receiver is characterized by its length, width, and spectral response curve. Finally, the electronics of the system are parameterized by a start time, a stop time, a time resolution, and gain factor. Additional parameters may be incorporated as the model is extended and validated against real data.

V. RESULTS

The results are presented in this section and discussed qualitatively. Validation experiments are being planned to quantitatively evaluate both the CCD and LIDAR models.

A. CCD model

An image produced by the sensor model described in the first section is shown in Fig. 3 and compared to the real image in Fig. 4. Several features of the camera model are evident in these images, including the vignetting near the lower left and right corners of the simulated image, the detailed shadows produced by a gamma setting of 0.5 in the camera model, and the slight distortion of the shape of the horizon due to optical effects. The qualitative agreement between the images gives a good indication that the basic features of the model are correct.

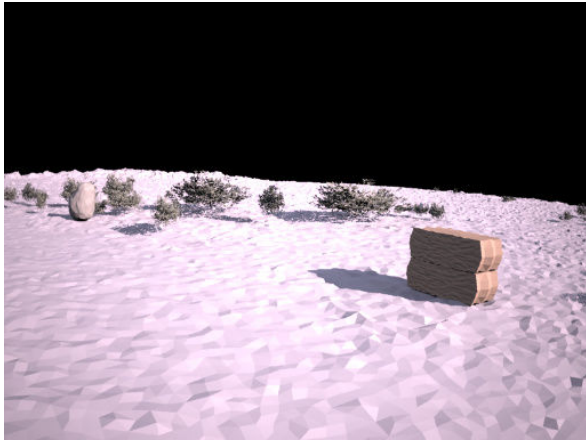


Fig. 3. Simulated image taken with a software model of the Bumblebee.

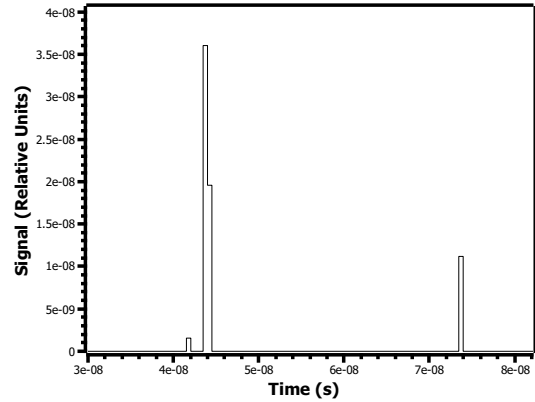


Fig. 4. Real image taken with the Point Grey Bumblebee RGB camera with Sony ICX204 CCD.

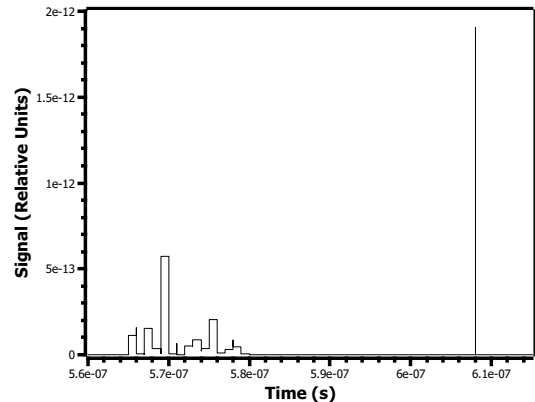
B. LIDAR model

An example of a pulse vs time curve as produced by the LIDAR model is shown in Fig. 5. These pulses are simulated

by using the geometry depicted in Fig. 6, which is a bush in front of a solid wall. The top figure is a single pulse taken at 6 m, while the bottom shows a pulse from 86 m. Both signals show an initial return from the bush, followed by a small amount of scattering from the wall behind the bush.



(a) LIDAR return pulse from the bush at 6 m.



(b) LIDAR return pulse from the bush at 86 m.

Fig. 5. Example of LIDAR returns at 6 m and 86 m from the bush shown in Fig. 6.

There are several interesting points of comparison between Fig. 5(a) and Fig. 5(b). First, there is roughly a factor of 10^4 decrease in signal strength from 6 m to 86 m, which is to be expected from (9). Second, the signal from the more distant scan is also relatively more complex. This complexity is due to the much increased beam spot size at this distance. With a divergence of 10 mrad, the beam has a diameter of 88 cm for the 86 m scan, nearly covering the entire bush. The beam diameter for the pulse from 6 m is only 8.5 cm, covering only a small portion of the bush.

VI. CONCLUSION AND FUTURE WORK

We have developed a semi-generic model of both a LIDAR and a CCD camera. These sensor models will be used to provide input for autonomous mobility systems as part of the VANE. A signal processing algorithm to extract distance from the LIDAR pulse will be added to the model, and validation of both the LIDAR and CCD models against real sensor data is being initiated.

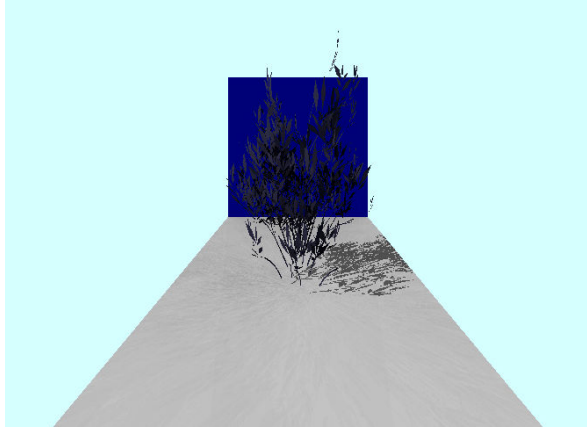


Fig. 6. Geometry of the bush and wall used to test the LIDAR model. Note that this image is an ideal image from the ray caster.

ACKNOWLEDGMENT

Permission to publish was granted by Director, Geotechnical and Structures Laboratory, ERDC.

REFERENCES

- [1] J. F. Peters, J. R. Ballard, S. E. Howington, and L. N. Lynch, "Signature Evaluation for Thermal Infrared Countermeasure and IED Detection Systems," in *Proceedings of the 2007 High-Performance Computing Users Group Conference*, 2007, pp. 238–246.
- [2] M. Subbarao and A. Nikzad, "Model for image sensing and digitization in machine vision," in *Proceedings of SPIE*, vol. 1385. SPIE, 1991, p. 70.
- [3] M. Born and E. Wolf, *Principles of Optics*, 6th ed. Elmsford, New York: Pergamon Press, 1980.
- [4] H.-C. Lee, "Review of image-blur models in a photographic system using the principles of optics," *Optical Engineering*, vol. 29, no. 5, pp. 405–409, 1990.
- [5] S. Kang and R. Weiss, "Can we calibrate a camera using an image of a flat, textureless Lambertian surface?" in *Computer Vision - ECCV 2000*, vol. 1843, 2000, pp. 640–653.
- [6] J. Tuley, N. Vandapel, and M. Hebert, "Analysis and Removal of artifacts in 3-D LADAR Data," in *Robotics and Automation, 2005. ICRA 2005. Proceedings of the 2005 IEEE International Conference on*, 2005, pp. 2203–2210.
- [7] L. Rong, W. Chen, S. Yu, and W. Song, "Mathematical model of coordinate transformations for 3D Depth-of-field collection system," in *6th IEEE International Conference on Industrial Informatics, 2008. INDIN 2008*, 2008, pp. 80–85.
- [8] B. M. Sabol, J. R. Ballard, and T. A. DeMoss, "Description, Verification, and Validation of a Laser Profilometer Simulation Model for the Advanced Hornet Suble Sensor," Environmental Laboratory, US Army ERDC, Tech. Rep. TR-03-16, 2003.